Minimum radiative heat-load aerocapture guidance with attitude-kinematics constraints

Zucchelli, E. M.; Mooij, E.

DOI
10.2514/6.2018-1319

Publication date
2018

Document Version
Accepted author manuscript

Published in
AIAA Guidance, Navigation, and Control Conferenc

AIAA-18-1319

Minimum Radiative Heat-load Aerocapture Guidance with Attitude-Kinematics Constraints

E. Zucchelli and E. Mooij and D.I. Gransden
Delft University of Technology, Delft, The Netherlands

AIAA Guidance, Navigation, and Control Conference
January 8-12, Kissimmee, FL

Minimum Radiative Heat-load Aerocapture Guidance with Attitude-Kinematics Constraints

E.M. Zucchelli* and E. Mooij†

Delft University of Technology, Faculty of Aerospace Engineering,

Kluyverweg 1, 2629 HS Delft, The Netherlands

To maximize the payload mass, an aerocapture trajectory should be flown in such a way that both the final ΔV and the total heat load are minimized. At very high velocities, the heating due to radiation of high temperature gases in the shock-layer exceeds the heat due to convection. For some aerocapture missions, such a heat load can be 15 times larger than the heat load due to convection. Thus, convective heat load may in some cases be neglected. It is analytically proven that radiative heat load is minimized by the same trajectory that minimizes the final ΔV: a bang-bang trajectory, with full lift-up, full lift-down commands. Next, a novel guidance that plans a bang-bang trajectory with constraints in the attitude kinematics is introduced. This allows for achieving an optimal trajectory with only one parameter to be tuned. For the case studied, values of ΔV as low as 100 m/s can be ensured for entry angles between -6° and -5° and a large spectrum of perturbations; with the same guidance, radiative heat load is reduced by up to 20% with respect to traditional aerocapture-guidance methods. Finally, a lateral guidance that makes use of information on the final inclination of the predicted trajectory is introduced. Such guidance allows for very high accuracy in the inclination requirements with only two reversals, and also requires only a single parameter to be tuned. Depending on the tuning, a maximum inclination error of less than 0.1° can be guaranteed.

Nomenclature

a	semi-major axis, m
C_D	drag coefficient
C_L	lift coefficient
D	drag, N
e	eccentricity
g_δ	latitudinal component of the gravity, m/s^2
g_r	radial component of the gravity, m/s^2
i	inclination, rad
L	lift, N
m	mass, kg
$\dot{q}$	heat flux at stagnation point, W/s^2
Q	integrated heat load, J/s^2
r	radial distance, m
R_e	equatorial radius of the Earth, m
R_N	nose radius, m
t	time, s
V	relative speed, m/s
β	inverse of scale-height, 1/m
γ	relative flight-path angle, rad
δ	latitude, rad

*MSc Graduate Student, Section Astrodynamics and Space Missions.

†Assistant Professor, section Astrodynamics and Space Missions, e.mooij@tudelft.nl, Associate Fellow AIAA.

λ	co-state
μ	gravitational parameter of the Earth, m^3/s^2
ρ	atmospheric density, kg/m^3
σ	bank angle, rad
τ	longitude, rad
χ	heading, rad
ω_{cb}	rotational rate of the Earth, rad/s

Subscripts

0	initial conditions
a	apoapsis
m	margin
p	periapsis
$pred$	end of prediction
rev	reversal
opt	optimal

Superscripts

$\star$	target

I. Introduction

Aerocapture is a maneuver to achieve orbit insertion; the energy of the spacecraft is reduced in a controlled way using the dissipative action of drag, obtained by diving into the atmosphere. A small propulsive burn is then required to raise the periapsis, and, in most cases, a second burn is needed to correct the apoapsis altitude.

Aerocapture was first introduced in Ref. 1. Since then, it has never been attempted in practise, despite the fact that most of the necessary component technologies have been ready for some years now.[2] Reference 3 compares aerocapture to other capture methods, and shows that in the majority of the proposed scenarios it is the technology that allows the largest payload-mass increase. At the current state of technology, aerocapture is the only viable option to orbit Neptune, or to have low circular orbits around Jupiter.

Optimality has rarely been considered in closed-loop aeroassisted problems. Concerning open-loop optimization, Ref. 4 showed numerically that the optimal aerocapture, in terms of minimizing the final ΔV, is obtained by a bang-bang trajectory, beginning with a full lift-up command. Such results have been later proved analytically for a non-rotating planet.[5] It has also been numerically shown that the same trajectory that minimizes the final ΔV, minimizes both the heat-flux peak and the peak structural load.[6] However, Ref. 7 shows (both analytically and numerically) that such a trajectory *maximizes* the integrated, convective heat load, which is instead minimized by a bang-bang trajectory that begins with a full lift-down command.

In aerocapture, a major component of the heat load is due to the radiation of high-temperature gases in the shock layer. In this paper, it is analytically shown that such a component is minimized by the same trajectory that minimizes the ΔV. This is a very useful result, since heat flux due to radiation is comparable to convective heat flux for a lunar return aerocapture, and becomes much larger than that for even higher initial velocities, and for vehicles with larger nose radii. Figure 1 shows the radiative and convective heat flux in the stagnation point for an aerocapture flown into the Earth's atmosphere by Orion, with an entry velocity of 16 km/s and an entry angle of -8°. In that case, the radiative heat flux peak is 30 times larger than its convective counterpart; most importantly, radiative heat load is 15 times larger than the convective heat load. Hence, minimization of radiative heat load becomes much more important than minimization of convective heat load. For high speed aerocapture, one does not need to have trade offs between minimum heat load and minimum ΔV, since the same trajectory minimizes them both.

Optimal closed-loop guidance for an aeroassisted maneuver was first shown in Ref. 8. The underlying idea was to divide the maneuver into two phases. In the first phase, the algorithm would integrate a constant, quasi full lift-down trajectory. If the thus predicted apoapsis were lower than the desired one, a full lift-up would be commanded; else, phase 2 would be triggered, in which the algorithm would look for a constant bank angle that leads to apoapsis targeting. This method achieves optimality avoiding online trajectory

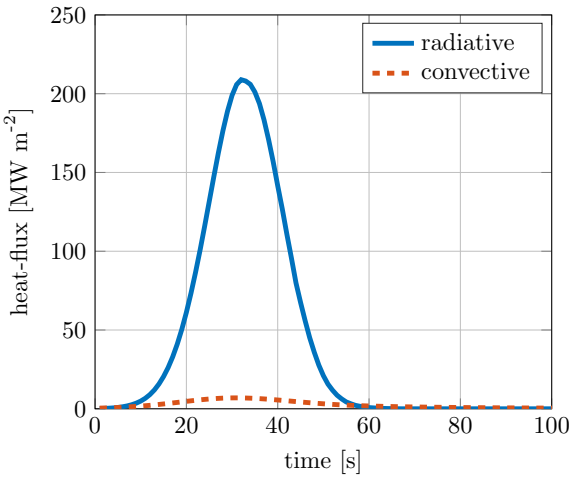

Figure 1: Stagnation point radiative and convective heat flux for aerocapture with γ_0 =-8°, V_0 =16 km/s.

optimization. It was noticed that a bank-angle margin was required, which would decrease performance, but reduce the risk of skipping out. Bank-angle margins were kept constant independently of the entry conditions. It was found that this choice leads to a decrease in performance for shallow entry flight-path angles. A similar method was used in Ref. 5, differing from the previous case that the method focussed on the switching time in phase 1, instead of just checking whether the trajectory is feasible. More importantly, though, the authors aimed to look for the optimal bank-angle margins as a function of entry conditions.

In the current paper, it is shown that the major reason why a different bank-angle margin is needed for different entry conditions is the unconstrained kinematics in the motion-planning of phase 1: the rotation from the bank angle of phase 1 to the bank angle in phase 2 occurs instantaneously in the planning of the guidance logics in Refs. 5 and 8. This is no exception, as in the majority of re-entry guidance logics, attitude kinematics are not considered in the planning. This makes sense, since rotations usually have a negligible duration with respect to the entire mission, and one can therefore usually assume time-scale separation between attitude and translational dynamics. One of the contributions of this paper is the realization that a guidance logic for aerocapture obtains large benefits if constraints in the attitude kinematics of the inner loop are included. The duration of the rotation between phase 1 and 2 is approximately 10 seconds. As shown in Fig. 2, in ten seconds of aerocapture, more than 20% of the difference in energy between initial and final states can be dissipated. At maximum dynamic pressure, up to 0.7 MW/kg may be dissipated, out of a total energy difference of 32 MJ/kg. These numbers vary depending on when the rotation occurs during the mission, as well as on the initial entry conditions. Consequently, it is very important that a planner captures such motion. The guidance proposed in this paper leads to a performance similar to that of Ref. 5, but using the minimal tuning of Ref. 8.

Eventually, a robust lateral guidance with only one parameter, the inclination margin, or i_m, is proposed. This guidance logic aims to minimize the number of bank reversals. It can do so by making use of the inclination predicted at the end of each guidance cycle, as well as additional information obtained from the propagation of the trajectory.

Summarizing, the contributions of this paper can be listed as follows:

1. The analytical proof that the minimum radiative heat-load aerocapture is the same one that leads to a minimum ΔV. For very high-velocity aerocapture, convective heat flux is much smaller than the radiative one; thus, that same trajectory would minimize the total integrated heat load as well. This is in contrast to the trajectory that minimizes the integrated convective heat load only.

2. A new optimal numeric predictor-corrector (NPC) for longitudinal aerocapture guidance that achieves optimal results with minimal tuning, by constraining the attitude kinematics in the planning.

3. Strictly related to the previous item, is the finding that time-scale separation between attitude and translational dynamics is not a valid assumption in aerocapture.

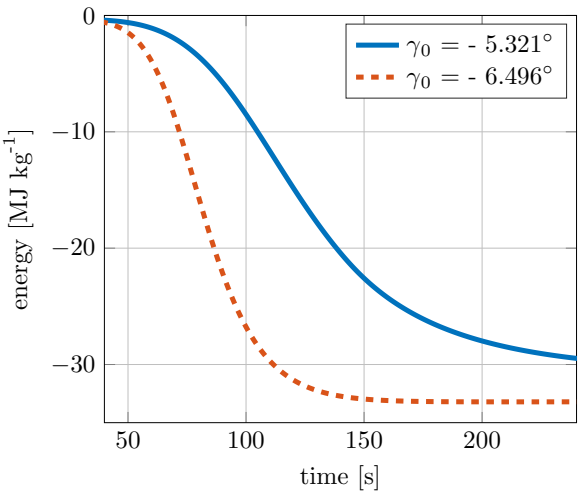

Figure 2: Specific energy versus time for Lunar-return conditions, aerocapture with shallow and steep entry angles, flown with constant bank angle.

4. A new lateral guidance that makes use of the lateral conditions computed at the end of the prediction of each cycle. Such a guidance has been partly tailored to the longitudinal guidance proposed in this paper, but is easily applicable to other entry problems.

To this end, Sec. II describes the dynamics of aerocapture, and gives the analytical proof of the trajectory minimizing radiative heat load. Section III introduces both the longitudinal and the lateral logics of the novel guidance of this paper. Section IV shows the results obtained from an extensive simulation campaign. The guidance is tested for different conditions and vehicles. Particular attention is also given to the analysis of the heat load. Section V concludes this paper.

II. The Aerocapture Maneuver

A. Equations of Motion

During aerocapture, the dynamics of the vehicle are dominated by gravitational and aerodynamic forces. Including the J_2 component of the gravity field, the equations of motion of a vehicle in the atmosphere of a planet are, in spherical coordinates, in a planet fixed reference frame:[9]

$$\dot{V} = -\frac{D}{m} - g_r \sin\gamma - g_\delta \cos\gamma \cos\chi + \omega_{cb}^2 r \cos\delta(\sin\gamma\cos\delta - \cos\gamma\sin\delta\cos\chi) \tag{1}$$

$$V\dot{\gamma} = \frac{L\cos\sigma}{m} - g_r\cos\gamma + g_\delta \sin\gamma\cos\chi + 2\omega_{cb}V\cos\delta\sin\chi + \frac{V^2}{r}\cos\gamma + \\ + \omega_{cb}^2 r\cos\delta(\cos\gamma\cos\delta - \sin\gamma\sin\delta\cos\chi) \tag{2}$$

$$V\cos\gamma\dot{\chi} = \frac{L\sin\sigma}{m} + g_\delta\sin\chi + 2\omega_{cb}V(\cos\gamma\sin\delta - \sin\gamma\cos\delta\cos\chi) + \\ + \frac{V^2}{r}\cos^2\gamma\tan\delta\sin\chi + \omega_{cb}^2 r\cos\delta\sin\delta\sin\chi \tag{3}$$

$$\dot{r} = V\sin\gamma \tag{4}$$

$$\dot{\tau} = \frac{V\sin\chi\cos\gamma}{r\cos\delta} \tag{5}$$

$$\dot{\delta} = \frac{V\cos\gamma\cos\chi}{r} \tag{6}$$

where V is the relative velocity, γ is the relative flight-path angle, χ is the relative heading angle, r is the radial distance from the center of the planet, and τ and δ are the longitude and latitude, respectively. L and

D are the aerodynamic lift and drag, m is the vehicle mass, ω_{cb} is the planet angular velocity, and σ is the bank angle. g_r and g_δ are the two components of the gravity field, when the J_2 zonal term is included:

$$g_\delta = -\frac{3}{2}\mu J_2 \frac{R_e^2}{r^4} \sin 2\delta \tag{7}$$

$$g_r = \frac{3}{2}\mu J_2 \frac{R_e^2}{r^4} \left(3\sin^2\delta - 1\right) \tag{8}$$

Standard coordinate transformations can link the above model to Keplerian orbits. Given a target circular orbit with semi-major axis a^*, and assuming an exit orbit with semi-major axis a and apoapsis $r_a = a(1+e)$, the magnitude of planar ΔV, required to raise the periapsis, as well as to correct the apoapsis, is:[5]

$$\Delta V = \|\Delta V_1\| + \|\Delta V_2\| = \sqrt{2\mu}\left(\left\|\sqrt{\frac{1}{r_a} - \frac{1}{r_a + a^\star}} - \sqrt{\frac{1}{r_a} - \frac{1}{2a^\star}}\right\| + \left\|\sqrt{\frac{1}{2a^\star}} - \sqrt{\frac{1}{a^\star} - \frac{1}{r_a - a^\star}}\right\|\right) \tag{9}$$

This equation can easily be generalized to elliptical target orbits. However, this case will not be treated here, since circular target orbits benefit most from aerocapture.

The ΔV needed because of a change in inclination is:

$$\Delta V_i = 2V \sin(\frac{\Delta i}{2}) \tag{10}$$

Finally, the total ΔV_{tot}, that includes in-plane and out-of-plane components, is:

$$\Delta V_{tot} = \sqrt{\Delta V_1^2 + \Delta V_i^2} + \Delta V_2 \tag{11}$$

The out-of-plane correction is assumed to be occurring entirely during the first burn. The optimal strategy would be to leave a small portion of the correction for the second burn. Nonetheless, the difference would be negligible.

B. Minimum Radiative Heat-load Aerocapture

It is possible to infer some analytical conclusions on the optimal aerocapture trajectory if a non-rotating planet is assumed, and if there are no requirements on the final inclination. In such a case, an aerocapture leads to a minimum ΔV if the bank-angle history is full lift-up, full lift-down.[5] Conversely, an aerocapture leads to minimum integrated convective heat flux if the bank-angle history is full lift-down, full lift-up.[7] The two objectives thus lead to opposite trajectories. Nonetheless, during aerocapture a major source of heat flux comes from the radiation of incandescent gases in the shock-layer. For lunar entry conditions, the total radiative heat load is comparable to the total convective heat load. For even higher velocities, the ratio changes in favor of the radiative heat load. For entry velocities of 16 km/s, the radiative heat load is 6 to 12 times larger than the convective heat load. Thus, minimization of radiative heat load becomes much more important than minimization of the convective heat load. It is the objective of this section to prove that the integral of (almost) any monomial function of density and velocity is minimized by a bang-bang trajectory. For empirical formulations of the radiative heat flux,[10,12] such a trajectory is full lift-up, full lift-down, which corresponds to minimizing ΔV, the heat-flux peak, and the load-factor peak.

Given a function $f = f(\rho, V)$, where $\rho = \rho_0 e^{\beta h}$ is assumed to follow an exponential profile; β is the inverse of the scale height. For a spherical, non-rotating planet, Eqs. (1) to (6) reduce to:

$$\dot{V} = -\frac{D}{m} - g\sin\gamma \tag{12}$$

$$V\dot{\gamma} = \frac{L\cos\sigma}{m} - g\cos\gamma + \frac{V^2}{r}\cos\gamma \tag{13}$$

$$\dot{r} = V\sin\gamma \tag{14}$$

The cost function to be minimized is:

$$J = \int_{t_0}^{t_f} f(\rho, V) \tag{15}$$

The corresponding Hamiltonian is:

$$H = f(\rho, V) + \lambda_r V \sin\gamma + \lambda_V \left(-D - \frac{\mu \sin\gamma}{r^2}\right) + \lambda_\gamma \left[\frac{L}{V}\cos\sigma + \left(V^2 - \frac{\mu}{r}\right)\frac{\cos\gamma}{rV}\right] \tag{16}$$

where, according to the Pontryagin Maximum Principle:[11]

$$\dot{\lambda}_r = -\frac{\partial H}{\partial r} = \rho\beta\frac{\partial f(\rho, V)}{\partial \rho} + \lambda_V\left(\frac{\partial D}{\partial r} - \frac{2\mu\sin\gamma}{r^3}\right) - \lambda_\gamma\frac{\partial\dot{\gamma}}{\partial r} \tag{17}$$

$$\dot{\lambda}_V = -\frac{\partial H}{\partial V} = -\frac{\partial f(\rho, V)}{\partial V} - \lambda_r\sin\gamma + \lambda_V\frac{\partial D}{\partial V} - \lambda_\gamma\frac{\partial\dot{\gamma}}{\partial V} \tag{18}$$

$$\dot{\lambda}_\gamma = -\frac{\partial H}{\partial\gamma} = -\lambda_r V\cos\gamma + \lambda_V\frac{\mu\cos\gamma}{r^2} - \lambda_\gamma\frac{\partial\dot{\gamma}}{\partial\gamma} \tag{19}$$

The optimal bank angle σ_{opt} has to be such that, at any moment, the Hamiltonian H is maximized:

$$\sigma_{opt} = \arg\max_\sigma \left\{f(\rho, V) + \lambda_r V\sin\gamma + \lambda_v\left(-D - \frac{\mu\sin\gamma}{r^2}\right) + \lambda_\gamma\left[\frac{L}{V}\cos\sigma + \left(V^2 - \frac{\mu}{r}\right)\frac{\cos\gamma}{rV}\right]\right\} \tag{20}$$

Since $\cos\sigma$ is monotonic in $\sigma \in [\sigma_{min}, \sigma_{max}]$, and $L/V > 0$, the optimal bank angle can be different from its extrema only if a singular arc exists, which requires $\lambda_\gamma \equiv 0$. It will be proven by contradiction that this cannot happen. For λ_γ to be constant and equal to zero for a finite time, it is required to have $\lambda_\gamma = \dot{\lambda}_\gamma = 0$; all higher derivatives should also be equal to zero. This implies, substituting $\lambda_\gamma = 0$ in Eq. (19):

$$\lambda_V\frac{\mu}{r^2} - V\lambda_r = 0 \tag{21}$$

since $\cos\gamma \neq 0$ (for a lifting body, $\cos\gamma = 0$ is not a physically realistic situation). Because the Hamiltonian does not explicitly depend on time, and the final time is free, $H \equiv 0$ holds for the entire trajectory. Thus, the existence of a singular arc would imply:

$$f(\rho, V) + \lambda_r V\sin\gamma - \lambda_V D - \lambda_V\frac{\mu\sin\gamma}{r^2} = 0 \tag{22}$$

Substituting Eq. (21), Eq. (22) reduces to:

$$f(\rho, V) - \lambda_V D = 0 \tag{23}$$

such that the costates can be expressed as:

$$\lambda_V = \frac{f(\rho, V)}{D} \tag{24}$$

$$\lambda_r = \frac{\mu f(\rho, V)}{r^2 DV} \tag{25}$$

A singular arc requires that also all higher derivatives of the costate variable are zero. Thus, also $\ddot{\lambda}_\gamma = 0$. Taking the time derivative of Eq. (19) yields:

$$\ddot{\lambda}_\gamma = \left[\dot{\lambda}_V\frac{\mu}{r^2} - \lambda_V\frac{2\mu}{r^3}\dot{r} - \dot{\lambda}_r V - \lambda_r\dot{V}\right]\cos\gamma - \dot{\gamma}\sin\gamma\frac{\dot{\lambda}_\gamma}{\cos\gamma} = 0 \tag{26}$$

Because the arc is supposed to be singular, $\dot{\lambda}_\gamma = 0$; also, as was already established above, $\cos\gamma \neq 0$, which further simplifies the above equation. Substituting $\dot{\lambda}_V$ and $\dot{\lambda}_r$ together with λ_V and λ_r, obtained from Eqs. (24) and (25), and $\dot{V}$ and $\dot{r}$, Eqs. (12) and (14), results in:

$$\begin{aligned} -\frac{\partial f(\rho, V)}{\partial V}\frac{\mu}{r^2} - \frac{\mu^2 f(\rho, V)}{r^4 DV}\sin\gamma + \frac{2f(\rho, V)}{V}\frac{\mu}{r^2} - \frac{f(\rho, V)}{D}\frac{2\mu}{r^3}V\sin\gamma - \frac{\partial f(\rho, V)}{\partial\rho}\beta\rho V + \\ + \beta f(\rho, V)V + \frac{f(\rho, V)}{D}\frac{2\mu}{r^3}V\sin\gamma + \frac{\mu f(\rho, V)}{r^2 V} + \frac{\mu^2 f(\rho, V)}{r^4 DV}\sin\gamma = 0 \end{aligned} \tag{27}$$

This relation naturally reduces to:

$$\frac{\mu}{r^2}\left(\frac{\partial f(\rho,V)}{\partial V}-\frac{3f(\rho,V)}{V}\right)+\beta\rho V\left(-\frac{\partial f(\rho,V)}{\partial \rho}+\frac{f(\rho,V)}{\rho}\right)=0 \tag{28}$$

At this point, it can be noticed that a singular arc is possible if:

$$\frac{\partial f(\rho,V)}{\partial \rho}=\frac{f(\rho,V)}{\rho} \quad \wedge \quad \frac{\partial f(\rho,V)}{\partial V}=3\frac{f(\rho,V)}{V} \tag{29}$$

This implies $f(\rho,V)=\rho V^3$, which is not the case.

Otherwise, when assuming a general monomial form for the radiative heat:

$$f(\rho,V)=c\rho^m V^n \tag{30}$$

in which case Eq. (28) becomes:

$$c\left[\frac{\mu}{r^2}\left(3\rho^m V^{n-1}-n\rho^m V^{n-1}\right)+\beta\rho V\left(\rho^{m-1}V^n-m\rho^{m-1}V^n\right)\right]=0 \tag{31}$$

Dividing both sides by $c\rho^m V^{n-1}$:

$$(3-n)\frac{\mu}{r^2}=(m-1)\beta V^2 \tag{32}$$

Since $\mu/r^2\approx g_0$ is approximately constant, this equation implies a trajectory with constant velocity, which is impossible for non propelled, high-speed, flight. This is true for any monomial function, except for $n=3$ and $m=1$, which is the same case as before. Convective heat flux has $n=3$ and $m=0.5$, and thus this proof includes what has been proved in Ref. 7.

An additional insight is obtained by noticing that, in aerocapture, $\frac{\mu}{r^2}\ll\beta V^2$: as a consequence, changes in n are almost negligible if compared to changes in m. Thus, the sign of Eq. (31), and hence the order of commands, only depends on m: if $m>1$, the cost function will be minimized by a full lift-up, full lift-down trajectory; otherwise the opposite will occur. If one uses Martin's approximation for radiative heat flux:[12]

$$\dot{q}_{rad}\propto R_n\,\rho^{1.6}\,V^{8.5} \tag{33}$$

then it is shown that the radiative heat load along the entire trajectory is minimized by a bang-bang trajectory as well. Because $m>1$, the order of commands is full lift-up, full lift-down. It is possible to draw similar conclusions if the Tauber-Sutton relation is considered.

For the sum of convective and radiative heat flux, the situation becomes more complex. The extension of this proof to any polynomial follows. Given a polynomial of N terms, the condition for the existence of a singular arc is:

$$\sum_{i=1}^{N}c_i\rho^{m_i}V^{n_i-1}\left[(3-n_i)\frac{\mu}{r^2}+(1-m_i)\beta V^2\right]=0 \tag{34}$$

At this point, there may exist some parametric trajectories $\rho=f(V)$ such that Eq. (34) is satisfied, even if for just a short leg. Nonetheless, this is surely not possible for the entire aerocapture trajectory, since it has an ascending and a descending leg. This requires having two values of velocity for each value of density.

In conclusion, even though nothing can be said about the total heat load, the radiative heat load is minimized by a bang-bang trajectory with full lift-up and full lift-down commands. This is important, because radiation is already comparable to convective heat flux at low-speed aerocapture, and becomes the main heat source for aerocapture with large entry velocities, as well as for vehicles with large nose radii: for entry velocities of 16 km/s, the radiative heat load can be as large as 15 times the convective heat load.

C. Rotational Dynamics

A bang-bang trajectory involves a long lasting rotation, from the initial minimum bank angle to the maximum one (which, for reasons of robustness, is reduced to a value smaller than 180°). Assuming a maximum angular rate of 15°/s and a maximum angular acceleration of 5°/s^2, a rotation of 120° would take around 11 s. As previously shown in Fig. 2, in such time more than 20% of the total energy difference may be depleted. An additional problem consists of the fact that the rotation occurs at very different moments of the trajectory,

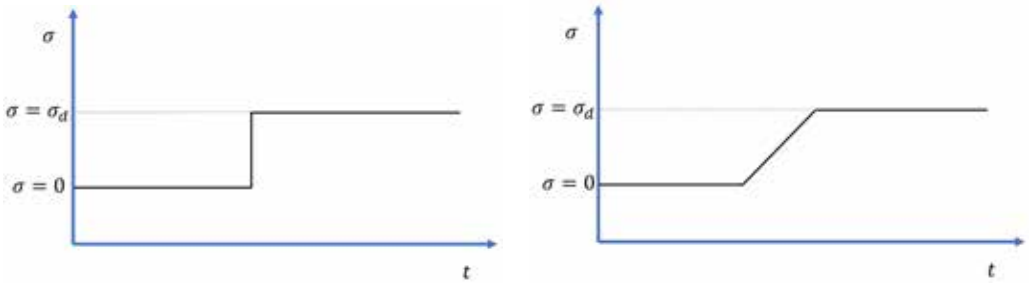

(a) Planning in Refs. 5 and 8.

(b) New planning.

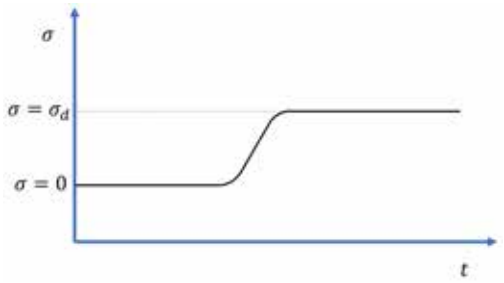

(c) Ideal planning.

Figure 3: Options for bank-angle planning for Phase 1.

depending on the entry conditions. For a shallow entry, the rotation occurs very soon, when dynamic pressure is small, and thus the error in modeling has small consequences. For a steeper entry, the rotation would occur later, when the dynamic pressure is larger, and thus causing larger errors in the prediction. Consequently, it is important for a guidance logic to include such a rotation in the trajectory planning. To begin with, the rotation has been modeled in the guidance as occurring with infinite angular acceleration, but with an average angular rate of $\dot{\sigma}_{exp}$ =10.5°/s. This approximation can already account for the majority of the error.

The rotational dynamics are less of an issue when having a bank inversion. In fact, independently of the angle at which the inversion starts, the inversion will end with an angle that is closer to 90° than the initial one. This leads to a small decrease in performance, but an increase in robustness at the same time.

III. Optimal Aerocapture Guidance with Attitude-Kinematics Constraints

The main novelty of the Optimal Aerocapture guidance with attitude-Kinematics constraints (OAK) consists of the inclusion of a simplified model for the rotation of the vehicle. Similarly to Ref. 5, the trajectory is divided into two phases.

A. Longitudinal Guidance

During Phase 1, the algorithm integrates the equations of motion using a bank-angle profile that varies linearly with rate $\dot{\sigma}_{exp}$ from the current bank angle to σ_d, and then remains constant. σ_d is the bank-angle value planned during Phase 1 to be used in Phase 2. If the so-predicted apoapsis is lower than the desired apoapsis, then the command does not change. Else, the command becomes equal to σ_d, and Phase 2 is triggered starting from the next guidance call. This causes a delay in the beginning of Phase 2 of no more than one sample time. Nonetheless, this phase requires only one iteration per guidance call, and thus the frequency can be increased, which reduces the delay. Figure 3 shows the difference between the planning of Phase 1 in previous works and the planning in the current work, as well as how an ideal planning should be.

During Phase 2, the logic iterates to find a constant bank angle that leads to the desired apoapsis. Given the very strong discontinuities, bisection is advised. This leads to obtaining an accuracy of 0.05° after only 13 iterations. Such an accuracy is higher than the implemented deadband.

In both phases, density filters are implemented as in Ref. 5. In the inner loop, the modeled lift and drag are multiplied by the scale factors $\tilde{\rho}_L$, and $\tilde{\rho}_D$, respectively. Given ρ_L,

$$\rho_L = L/L^\star \tag{35}$$

where L is the sensed lift, and $L^\star$ is the lift according to the model, the corresponding scale factor $\tilde{\rho}_L$ is updated at each cycle, applying a low-pass filter:

$$\tilde{\rho}_L^{(n+1)} = \tilde{\rho}_L^{(n)} + (1-k)\left(\rho_L - \tilde{\rho}_L^{(n)}\right) \tag{36}$$

The same holds for $\tilde{\rho}_D$. In this research, a value of $k = 0.95$ has been used.

B. Lateral logic

The lateral logic is specific for this guidance scheme. During Phase 1, the bank angle is proportional to the current error in inclination.

Once Phase 2 begins, the initial sign of the bank angle is chosen such that the initial direction of the trajectory is towards reducing the current inclination error. During Phase 2, the trajectory is propagated with a bank angle opposite to the commanded one. This leads to a small, constant deviation in the longitudinal guidance, but causes great benefits to the lateral guidance.

Let Δi_{rev} be the approximated change in inclination that occurs during the reversal, *i.e.,* the shift from Phase 1 to Phase 2:

$$\Delta i_{rev} = \|i_{rev} - i_0\| \tag{37}$$

where i_{rev} is the predicted final inclination at time $t_{rev} = 2\min(\pi - \sigma, \sigma)/\dot{\sigma}_{exp}$. Because the reversal lasts a considerable part of the total maneuver, Δi_{rev} can be as large as 0.4°. This is a change that cannot be ignored, which motivates to include Δi_{rev} in the guidance logic. During the entirety of Phase 2, a bank inversion is triggered, when all of the following conditions are true:

1. the inclination error at the end of the predicted trajectory, i_{pred}, and the current inclination error, i_0, have opposite signs;
2. i_{pred} is smaller than i_m times the current inclination error plus $\Delta i_{rev}/2$, and
3. i_{pred} is larger than the maximum allowable inclination error.

By doing so, and by setting a proper margin i_m, the number of reversals can be limited to two. A too small margin may lead to large final errors in the inclination, whereas a too large margin would lead to additional reversals. Since the latter situation is less problematic, when in doubt a larger margin should be preferred to an excessively small one. If a maximum number of reversals is set, i_m is automatically set to 0 before the last reversal.

A schematic of the lateral guidance is given in Fig. 4. Once the predicted inclination (dashed line) becomes smaller in absolute sense than the sum of current inclination (multiplied by i_m) and $\Delta i_{rev}/2$ (dashdotted line), the reversal begins. The margin i_m is needed because of the many perturbations that may happen after the reversal. In this paper, a 2-reversal strategy with $i_m = 0.3$ is used.

IV. Simulation Results

Testing of the guidance was carried out using a simulator for atmospheric flight on Earth, that was built, verified, and validated. The simulator includes GRAM large-scale[a] density perturbations,[14] a second-order gravity model, and Orion and Apollo databases. The database for Orion is for trim conditions at hypersonic flight, and uncertainties in aerodynamic coefficients as in Ref. 15. Apollo is modeled in trim conditions as in Ref. 16; uncertainties of aerodynamic coefficients are uniform for Apollo, in a range of ±20%. No winds have been modeled. A bank-angle deadband of 0.1° has been implemented for both vehicles. Initial conditions are as given in Ref. 5, although one should realize that given small differences in the various

[a]The baseline atmosphere used is instead the U.S. Standard Atmosphere of 1976.

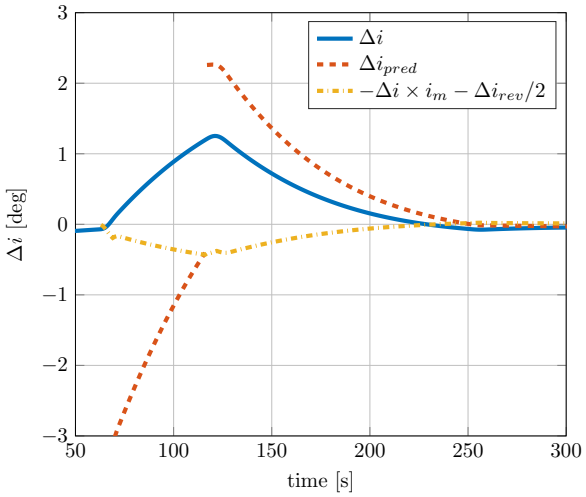

Figure 4: Schematic of the lateral logic during Phase 2; $i_m = 0.3$.

models and perturbation sets, some differences in the results are to be expected. The target orbit has an apoapsis altitude of 200 km, and an inclination of 90°. The guidance is triggered once a non-gravitational acceleration larger than 0.05 g is sensed. It is shut down when the spacecraft crosses 100 km altitude. The simulation is stopped once the apoapsis is reached. For all simulations, a maximum of two reversals has been chosen, together with an initial margin of 30%. This has given results that differ depending on the chosen value of σ_d. With $\sigma_d = 105°$, the maximum relative weight of the lateral ΔV is less than 1%, whereas with $\sigma_d = 135°$, the maximum relative weight grows to 15%. Consequently, it is clear that a different strategy should be chosen for higher σ_d.

A. Comparison with Previous Concepts

The comparison is divided into two parts. First, a conceptual difference is shown. In this case, the behavior of the guidance is evaluated in single, ideal cases; the comparison is done with respect to Mode 1 of the optimal aerocapture guidance[b] by Lu et al.[5] (which will be called, from here on, *Lu Mode 1*). The guidance is then compared in Monte Carlo simulations along a wide range of entry angles and perturbations. The comparison is with respect to *Lu Mode 1*, and Mode 6 of PredGuid+A.[17] PredGuid+A Mode 6 is a numerical predictor-corrector in which a constant bank angle is chosen at every iteration, such that the predicted apoapsis is equal to the target. Since *Lu Mode 1* requires an intensive interpolation that is vehicle and case dependent, such a comparison has to be carried out using Orion as reference vehicle. It has to be mentioned, though, that given the different perturbation settings, it may be that the optimal tuning for this case will be slightly different from the one of the original work. The tuning is obtained from interpolation of the data of Fig. 5.

Figure 6 shows the behavior of the bank angle under ideal conditions, with the *Lu Mode 1* guidance and the OAK guidance, respectively. In those cases, the environment is modeled exactly the same as in the guidance logic. The bank angle is optimally controlled (according to a minimum-time problem), constrained by maximum angular acceleration and velocity, and is not subjected to any perturbations. It is seen that even for such ideal conditions, using *Lu Mode 1*, the duration of the rotation is long enough to cause a major shift of the final bank angle. Moreover, such a shift depends on the initial entry angle. The reason is rather intuitive: an aerocapture with shallower entry angle will last longer and will be subjected to a smaller dynamic pressure than one with a steeper entry angle. Consequently, the effect of the rotation is less pronounced in the former case. This reasoning is in agreement with the optimal tuning obtained by Ref. 5 (shown in Fig. 5): in fact, the planned σ_d is larger for shallower entries, where the error caused is smaller; a larger margin is instead required for steeper entries.

The second part of the comparison consists of a Monte Carlo simulation, and is reported in Fig. 7. This is between *Lu Mode 1* and the OAK guidance with $\sigma_d = 120°$. Figure 7a shows that, in terms of apoapsis

[b]The guidance logic is not exactly the same. The main reason is the fact that the lateral logic proposed in this paper has been used.

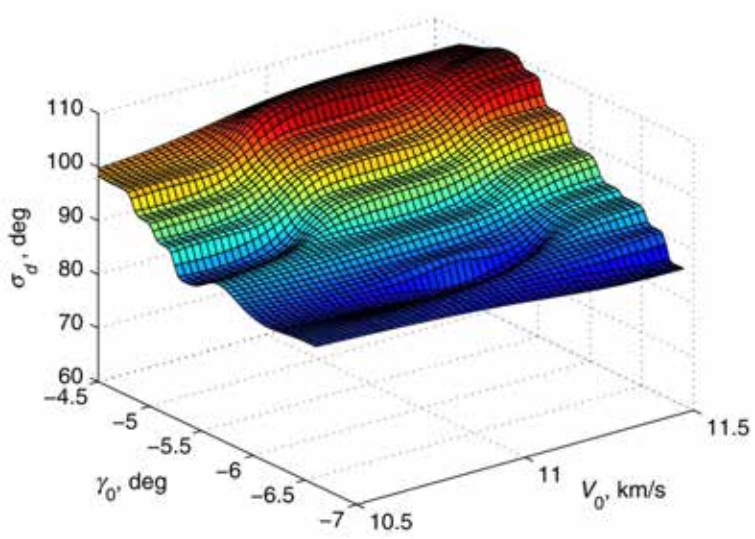

Figure 5: Manually determined best values of σ_d for Orion at different entry conditions.[5]

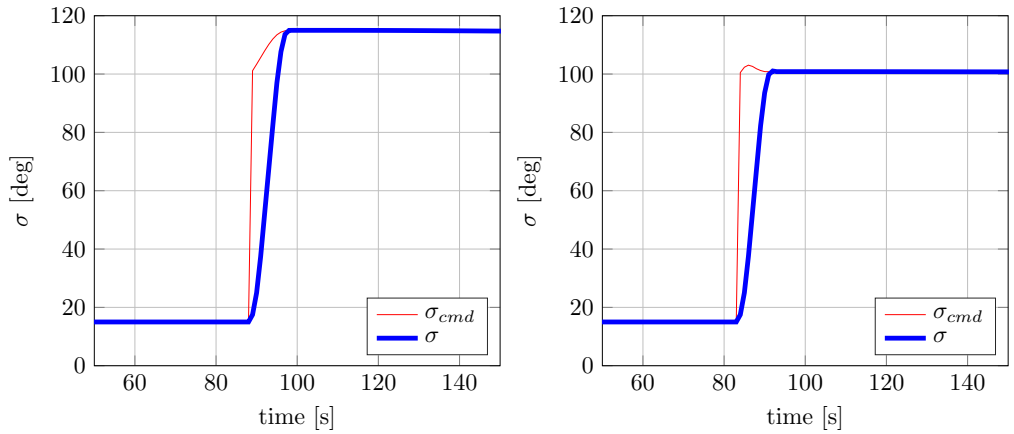

(a) *Lu Mode 1* (b) OAK

Figure 6: Bank-angle history during flight in ideal conditions, $\sigma_d = 100°$.

accuracy, the two concepts are rather similar. In Fig. 7b, the OAK guidance achieves slightly smaller values of ΔV for shallow entry angles. Nonetheless, such a difference might be due to other factors, such as the fact that the *Lu Mode 1* parameters are optimized for different conditions. Hence, it can be inferred that the two longitudinal logics are rather equivalent. The main difference consists of the fact that the *Lu Mode 1* guidance requires extensive hand tuning, whereas the OAK guidance can be set by defining a single parameter. In addition, the OAK guidance is conceptually more robust, as was previously shown.

It is interesting to compare the results of the OAK with PredGuid+A, Mode 6 (which is equivalent to OAK, with $\sigma_d = 0°$) as well. In terms of apoapsis accuracy the difference is rather evident. The PredGuid+A Mode 6 has errors in the range of -5 km and 0 km for steep entry flight-path angles, and between 0 and +10 km for shallow entry flight-path angles. OAK is more consistent, in that, as *Lu Mode 1*, has errors between 0 and +10 km for the entire range of entry angles. On average, PredGuid+A Mode 6 is more precise, but it has a larger uncertainty range. In terms of ΔV, OAK performs much better, as expected. For entry angles around -5.8°, the ΔV needed using PredGuid+A Mode 6 is around 200 m/s, approximately 2.5 times more than what is obtained with OAK for those same conditions. It is curious to notice the rightmost branch of the ΔV using PredGuid+A Mode 6. It is a strict consequence of the lateral logic. In fact, for the range of entry angles between -6.3° and -5.3°, the first bank reversal occurs when the bank angle is smaller

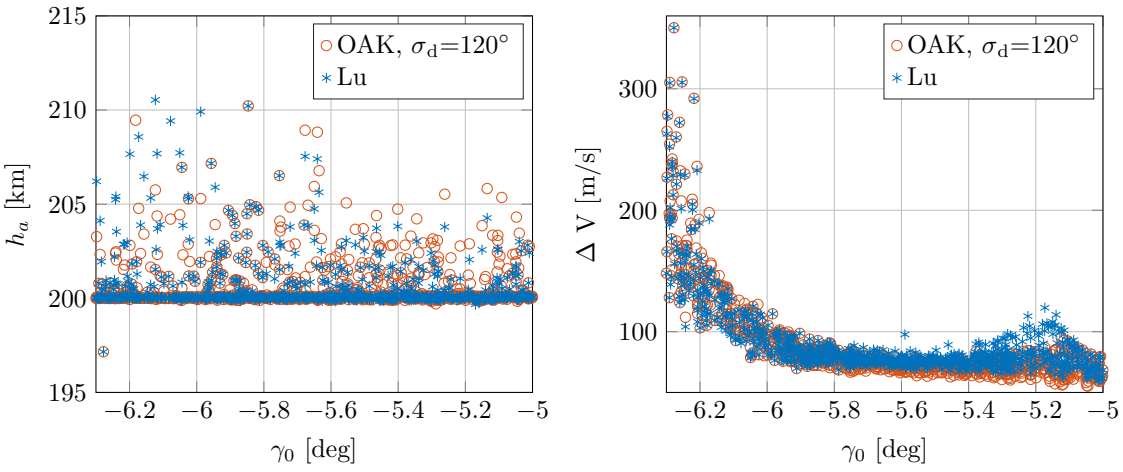

(a) Apoapsis altitude

(b) ΔV

Figure 7: Comparison between *Lu Mode 1* and OAK, $\sigma_d = 120°$.

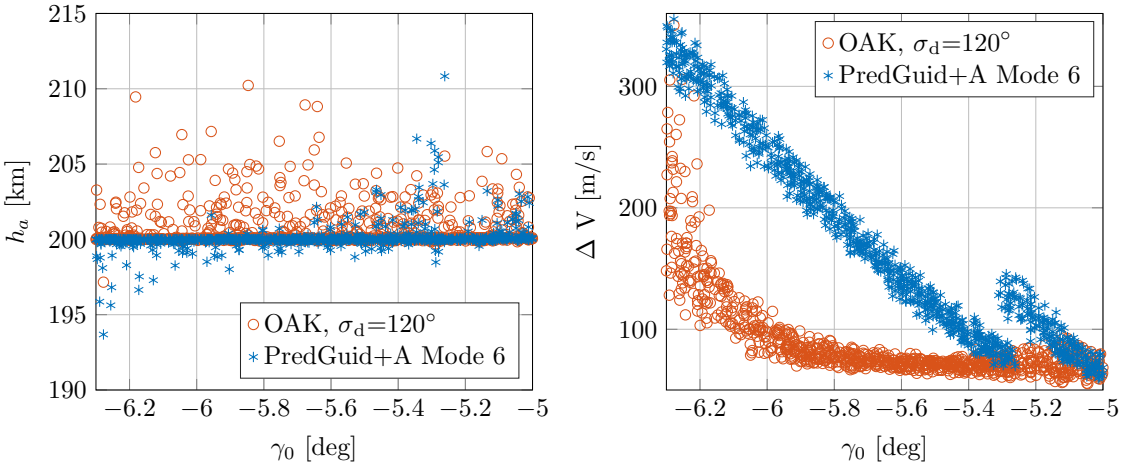

(a) Apoapsis altitude

(b) ΔV

Figure 8: Comparison between PredGuid+A Mode 6 and OAK, $\sigma_d = 120°$.

than 90°. As a consequence, the first rotation is upwards (because of the lateral logic being used, rotations after the first one have almost negligible effect on the longitudinal performance). This causes an increase in performance, for the same reason why a full lift-up, full lift-down trajectory is the optimal one. For shallower entry angles, the opposite happens, causing a sudden decrease in performance. Such a difference is never noticed in OAK. With $\sigma_d = 105°$ or larger, the rotation is always downwards. Nonetheless, it is also shorter, and affects the performance less (the larger the σ_d, the smaller, on average, the duration of the reversal). Although causing a decrease in performance, the reversal in the downward direction is often necessary. As a last remark, it is reasonable that for both very shallow and very steep initial flight-path angles, the two guidance logics perform the same. In those cases, not much room for optimality is left.

B. Sensitivity with respect to σ_d

It is interesting to analyze how a change in σ_d affects the performance of the guidance over the full range of entry conditions. After having shown that this new guidance logic achieves close-to-optimal performance, while making use of a single value of σ_d for a wide range of entry angles, the sensitivity with respect to this

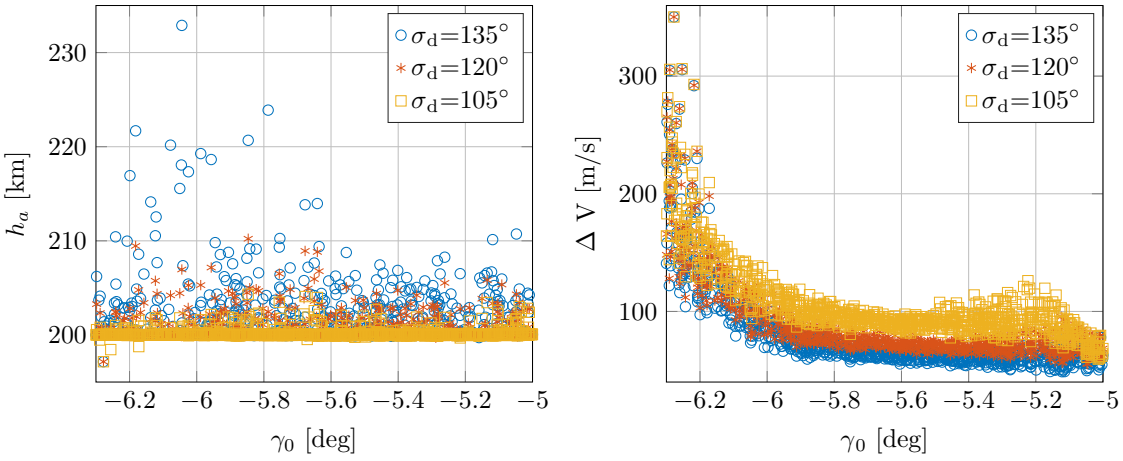

(a) Apoapsis altitude

(b) ΔV

Figure 9: Comparison between different values of σ_d for the OAK guidance.

parameter is now analyzed. Figure 9 shows apoapsis altitude and planar ΔV for the OAK guidance with three values of σ_d: 105°, 120°, 135°. While the one with the least margin performs best in terms of planar ΔV, it also causes the largest errors in apoapsis altitude (there is one outlier that is not shown in the figure, for σ_d = 135°, with γ_0 = -5.045°, and apoapsis altitude 268.7 km). These cases are caused by very early saturation. Unless it occurs extremely soon, saturation does not cause a sensible increase in planar ΔV, but prevents lateral control. This, in turn, gives large inclination errors that imply large out-of-plane corrections.

Table 1: Summary of OAK guidance systems longitudinal performances, for $\gamma_0 \in$ (-6°, -5°).

	In-plane ΔV [m/s]				$\|\Delta r_{apo}\|$ [km]	Δr_{apo} [km]			
σ_d [deg]	Mean	Min	Max	Std	Mean	Mean	Min	Max	Std
105	92.13	59.47	130.46	11.10	0.252	0.223	-0.476	4.328	0.590
120	74.21	55.19	114.74	49.1	0.698	0.677	-0.295	10.221	1.339
135	64.0	48.8	100.1	7.5	1.64	1.63	-0.28	68.73	3.70

Table 2: Summary of OAK guidance systems lateral performances, for $\gamma_0 \in$ (-6°, -5°).

	$\|\Delta i\|$ [°]	Δi [°]				ΔV_{tot} [m/s]			
σ_d [deg]	Mean	Mean	Min	Max	Std	Mean	Min	Max	Std
105	0.038	-0.023	-0.081	0.082	0.033	92.29	59.98	130.61	11.05
120	0.036	-0.023	-0.096	0.111	0.034	74.41	55.35	114.77	8.12
135	0.034	-0.018	-0.818	0.207	0.050	64.41	49.13	137.25	7.93

As a consequence, robustness should therefore be evaluated in terms of ΔV_{tot}, which is the ΔV required to correct orbit shape and plane at the same time. The maximum value of this parameter is an important spacecraft design parameter. The analysis is done for entry angles between -6° and -5°. In this range, the ΔV is approximately constant; outside of it, the difference in performance between the optimal aerocapture guidance and a simpler NPC reduces considerably. Tables 1 and 2 summarize the main performance parameters for the OAK guidance, with σ_d = 105°, 120°, and 135°. In terms of average values, the best performing guidance is the one with σ_d = 135°, both for what concerns in-plane and total ΔV. Nonetheless, it has a few cases in which the final inclination error is very large. This is caused by the fact that such value of σ_d leads to premature saturation, leaving no control authority to the lateral guidance. Such a result is in accordance with what is concluded in Ref. 5. Saturation happens also for lower values of σ_d, but it

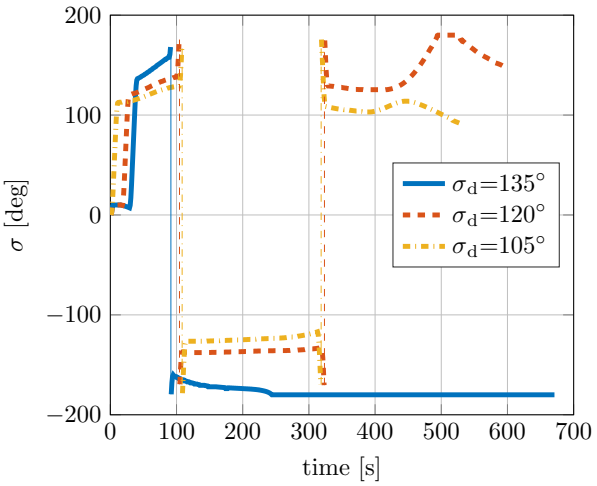

Figure 10: Bank angle history for OAK guidance with different values of σ_d, in a case of strong perturbations.

has a much smaller effect in the final inclination error. Figure 10 shows the bank-angle history of the three guidance logics for same conditions and perturbations. Where the one with highest σ_d saturates rapidly, leading to a final inclination error of more than 0.8°, the remaining two do not, leading to inclination errors of only 0.03° ($\sigma_d = 120°$) and 0.01° ($\sigma_d = 105°$).

It may very well be possible that by setting a larger inclination margin for the reversal, as well as a larger number of allowable reversals, the maximum total ΔV for σ_d may be reduced, and the logic be made more robust. Currently, the best trade-off between robustness and performance is given by OAK with $\sigma_d = 120°$, which can ensure a maximum total ΔV of 115 m/s.

C. Robustness to change of vehicle

At this point, it is analyzed whether the same parameter tuning can work on different vehicles. With this goal in mind, the performance of this guidance is analyzed using Apollo as a reference vehicle. Apollo has a 20% larger lift-to-drag ratio and a 7% smaller ballistic coefficient. The uncertainties in the coefficients have also been made very large (C_D and C_L both vary between ±20%, independently from each other), to further test the robustness of the guidance. Figure 11 shows the apoapsis altitude and planar ΔV for Apollo, in a slightly different range of initial flight-path angles. The figure shows a pattern very similar to the one of Orion. For Apollo as well, the worst case of ΔV_{tot} is best for $\sigma_d = 120°$, and is equal to 96.7 m/s; the worst case with $\sigma_d = 135°$ is 106.8 m/s instead. The difference between the two vehicles is not very large, but it is still interesting to see that the best σ_d is approximately the same for both.

D. Radiative Heat-load

It is already known from literature that a full lift-up, full lift-down trajectory maximizes the total convective heat load,[7] and minimizes the dynamic pressure and the convective heat-flux peaks.[6] The goal of this subsection is to show how a bang-bang trajectory behaves in terms of total heat load, specifically for the radiative component. This subsection is meant as a numerical confirmation of what was analytically proved in Sec. II.B. Here, the heat load of a set of trajectories flown with OAK guidance with $\sigma_d = 120°$ is compared with that obtained with a guidance that plans a constant bank angle for the entire trajectory (PredGuid+A Mode 6). Two formulations of radiative heat flux will be used, the one by Tauber and Sutton,[10] and the one by Martin.[12] A nose radius of 6.03 m has been used in the formulations. Even though this value exceeds the range of validity of the Tauber-Sutton formula, it still produces good results (and it is one of the most accepted formulas for estimation of radiative heat flux).

The convective, radiative (with Tauber-Sutton), and total heat load are shown in Fig. 12 for each of the simulated trajectories with OAK guidance. For steep entry angles radiative heat load is larger than the convective one; the opposite is true for shallow entry angles, which are closer to the case that maximizes

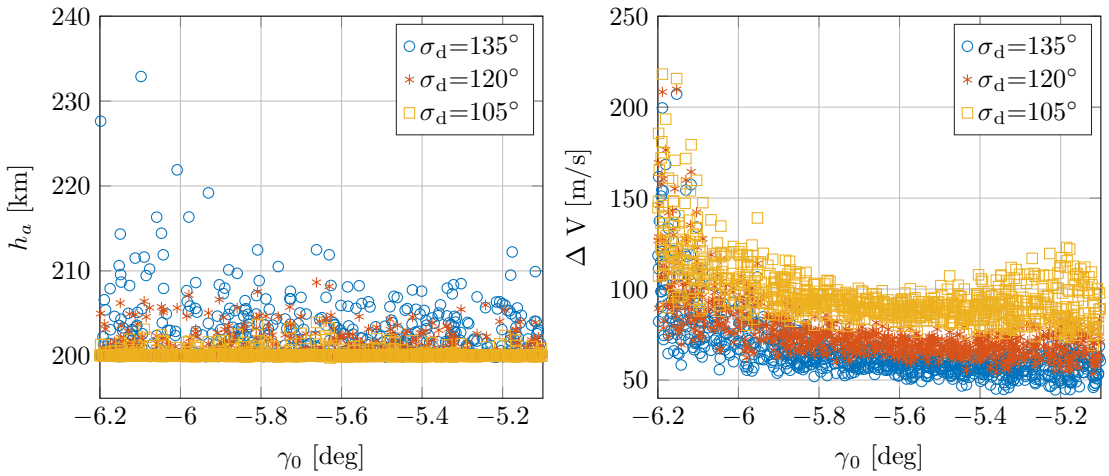

(a) Apoapsis altitude

(b) ΔV

Figure 11: Comparison between different values of σ_d for the OAK guidance.

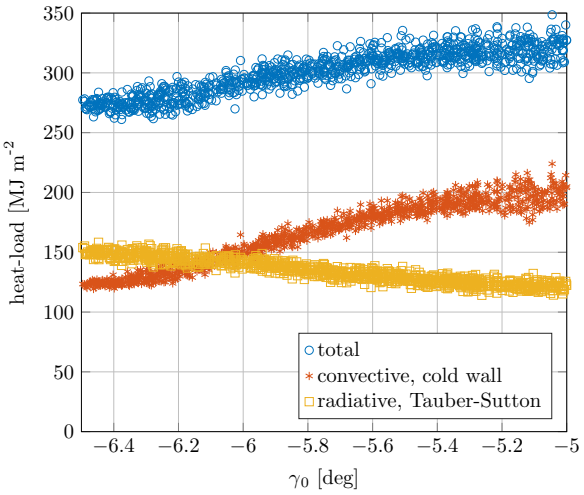

Figure 12: Heat-loads for dispersed conditions using the OAK guidance, $\sigma_d = 120°$.

convective heat load. Radiative heat load decreases mildly for shallow entry angles. It is expected that for larger entry velocities, the radiative heat load would become even more relevant. The ratio between the two heat sources is very dependent not only on entry conditions, but also on the vehicle itself. Whereas the convective heat load is proportional to $R_n^{-0.5}$, the radiative heat load is proportional to $R_n^{0.5}$ or even R_n. Therefore, for high-velocity aerocapture with large vehicles, one should aim to minimize the radiative heat load rather than the convective heat load. It is very fortunate that this same trajectory minimizes final ΔV, heat flux, load factor, and dynamic pressure peaks as well. Hence, when planning such a mission, one could reduce the problem of multi-objective, constrained optimization, to a single-objective, unconstrained optimization problem.

Figure 13 shows the ratio of different heat loads between same trajectories flown with OAK guidance, and PredGuid+A Mode 6. There is a symmetry between the convective heat load, and the radiative heat load computed with Martin's formula. Convective heat load is always larger for OAK, and radiative heat load is always smaller. With the Tauber-Sutton formula, the maximum reduction that can be obtained is about 5%, and is valid for only a very small range of entry angles, between -5.3° and -5.1°. Nonetheless, such a reduction may still be relevant, if the mission is such that the convective heat load is negligible with respect to the radiative one.

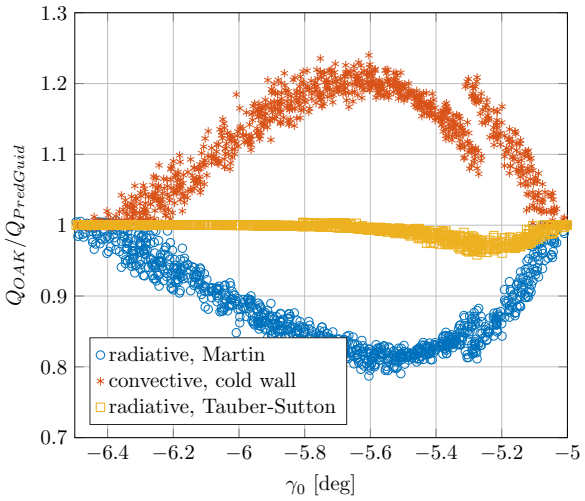

Figure 13: Ratio between heat load with OAK guidance ($\sigma_d = 120°$) and heat load with PredGuid+A Mode 6.

V. Conclusions and Recommendations

This paper brings four main contributions. First, there is the analytical proof that the aerocapture trajectory minimizing the ΔV also minimizes the radiative heat load. This is very important, because so far in literature only convective heat load has been considered when optimizing the aerocapture trajectory; convective heat load is instead maximized by such a trajectory. Moreover, for large vehicles and large entry velocities, convective heat load tends to be negligible with respect to radiative heat load: thus, the trajectory minimizing ΔV also minimizes the total heat load, in addition to minimizing heat flux, load factor, and dynamic pressure peaks.

The second one is the introduction of a new longitudinal guidance. This guidance achieves the same performance as that in Refs. 5 or 8, but it does so with much less tuning. For lunar entry conditions, and an apoapsis target altitude of 200 km, a ΔV of 100 m/s can be ensured for entry angles between -6° and -5°, and a large spectrum of perturbations

Third, the results obtained with this guidance make clear how important the rotational dynamics can be in the case of aerocapture. In most entry problems, one can separate the times scales of the translational motion and the rotational motion, because the latter is much faster than the former. This is not true in aerocapture, where up to 20% of the energy difference may be depleted, while rotating the spacecraft over 100°. Hence, the rotational dynamics have a major effect on the translational dynamics.

At last, a novel lateral guidance is introduced, that exploits the final inclination at the end of the trajectory. Such a lateral guidance, given an appropriate margin and maximum number of reversals, turns out to be very robust. When it fails, it is only due to a combination of too small margins with little robustness of the longitudinal guidance. With appropriate margins, this lateral guidance can guarantee a maximum inclination error of 0.082°. The correction for this inclination error requires no more than 4 m/s.

Recommendations for future work include the analysis of this guidance for different entry velocities, and how those affect the optimal choice of σ_d, as well as the total heat load. It is also recommended to use more appropriate approximations for the bank-angle rotation; the best option would be to use a sequence of first- and second-order functions, as shown in Fig. 3c. Such a planning has many discontinuities, though, which would make the integration more complex. A valid alternative could be the use of the (analytical) smooth step function, as done in Ref. 18 for a guidance that tracks path-constraints. Such a solution would give a less accurate approximation, but in a smoother and continuous way. The inclusion of the attitude kinematics is not a panacea, and the optimal σ_d is probably still dependent on the entry conditions. Nonetheless, such dependency is highly reduced, and a constant σ_d is very close to optimal.

Finally, it would be interesting to work on a Phase-2 guidance that, alternatively, seeks the constant bank angle at one guidance call, and the time of reversal at each second guidance call. This way, the rotation of the reversal could be more appropriately taken into account.

References

[1]Cruz, M. "The Aerocapture Vehicle Mission Design Concept", in: *Conference on Advanced Technology for Future Space Systems*, 1979.

[2]Munk, M., and Moon, S. "Aerocapture Technology Development Overview", in: *IEEE Aerospace Conference*, 2008.

[3]Hall, J., Noca, M., and Bailey, R. "Cost-Benefit Analysis of the Aerocapture Mission Set", in: *Journal of Spacecraft and Rockets*, Vol. 42, No. 2, 2005, pp. 309-320, 2005.

[4]Miele, A., Wang, T., Lee, W.Y., and Zhao, Z.G. "Optimal Trajectories for the Aeroassisted Flight Experiment.", in: *Acta Astronautica*, Vol. 21, No. 11/12, 1990, pp. 735-747.

[5]Lu, P., Cerimele, J.M., Tigges, M.A., and Matz, D.A. "Optimal Aerocapture Guidance.", in: *Journal of Guidance, Control, and Dynamics*, Vol. 38, No. 4, 2015, pp. 553-565.

[6]Miele, A., and Wang, T. "General Solution for the Optimal Trajectory of an AFE-Type Spacecraft.", in: *Acta Astronautica*, Vol. 26, No. 12, 1992, pp. 855-866.

[7]Sigal, E., and Guelman, M. "Aerocapture with minimum total heat.", in: *Proceedings of the 52nd International Astronautical Congress*, 2001.

[8]Evans, S. and Dukeman, G. "Examination of a Practical Aerobraking Guidance Algorithm.", in: *Journal of Guidance, Control, and Dynamics*, Vol. 18, No. 3, 1995, pp. 471-477.

[9]Miele, A., Zhao, Z., and Lee, W. "Optimal trajectories for the Aeroassisted Flight Experiment. Part 1: Equations of Motion in an Earth-fixed System.", 1989.

[10]Tauber, M., and Sutton, K. "Stagnation-point Radiative Heating Relations for Earth and Mars Entries", in: *Journal of Spacecraft and Rockets*, Vol. 28, No. 3, 1991, pp. 43-49.

[11]Pontryagin, L.S., Boltyanskii, V.G., Gramkreledze, Q.V., and Mishchenko, E.F. "The Mathematical Theory of Optimal Processes", Intersciences, New York, 1962.

[12]Martin, J.J. *Atmospheric Reentry: Introduction to its Science and Engineering.* Prentice-Hall Series in Space Technologies, Prentice-Hall, New Jersey, 1966

[13]National Aeronautics and Space Administration. "U.S. Standard Atmosphere, 1976", Technical Report NASA TM-X-74335, 1976.

[14]Leslie, F., and Justus, C. "The NASA Marshall Space Flight Center Earth Global Reference Atmospheric Model2010 Version", Technical Report NASA TM-2011-216467, 2011.

[15]Bibb, K. L., Walker, E. L., Brauckmann, G. J., and Robinson, P. E., "Development of the Orion Crew Module Static Aerodynamic Database, Part I: Hypersonic" AIAA Paper 2011-3506, *29th AIAA Applied Aerodynamics Conference*, Honolulu, Hawaii, 27-30 June, 2011.

[16]North American Aviation. "Aerodynamic Data Manual for Project Apollo", Technical Report NASA-CR-82907, 1965.

[17]Lafleur, J.M. "The Conditional Equivalence of ΔV Minimization and Apoapsis Targeting in Numerical Predictor-Corrector Aerocapture Guidance." NASA TM-2011-216156, 2011.

[18]Mooij, E. "Re-entry Guidance for Path-Constraint Tracking". In: *AIAA Guidance, Navigation, and Control Conference*, Grapevine, TX, 2017.